

# 5

## Quark Dynamics: the Strong Interaction

In Chapter 3 we described the basic properties of quarks and in particular their static properties and how these are used to construct the quark model of hadrons. We now look in more detail at how quarks interact and the role of gluons in the strong interactions. Thus we will be considering dynamical properties and the theoretical framework that describes these interactions.

### 5.1 Colour

We saw in Chapter 3 that the quark model account of the hadron spectrum is very successful. However, it begs several questions. One is: why are the observed states overwhelmingly of the form  $3q$ ,  $3\bar{q}$  and  $q\bar{q}$ ? Another arises from a particular assumption that was implicitly made in Chapter 3. This is: if two quarks of the same flavour  $uu$ ,  $dd$ ,  $ss \dots$  are in the same spatial state, they must also be in the same spin state, with their spins parallel. This can be seen very easily by considering the baryon state omega-minus  $\Omega^-$  that is shown in Table 3.3 and Figure 3.12.<sup>1</sup> From its decay products, it may be deduced that this state has strangeness  $S = -3$  and spin  $J = \frac{3}{2}$  and thus in the quark model it has the composition  $\Omega^- = sss$ , where all three quarks have their spins parallel and there is no orbital angular momentum between them. This means that all three like-quarks have the same space and spin states, i.e. the overall wavefunction must be symmetric, which violates the fundamental requirement of the Pauli principle. The latter states that a system of identical fermions has a wavefunction that is overall antisymmetric under the interchange of any two particles, because identical

---

<sup>1</sup>The discovery of the  $\Omega^-$  was a crucial step in gaining acceptance of the quark model of hadron spectroscopy. The experiment is described in Chapter 15 of Tr75.

fermions cannot simultaneously be in the same quantum state. The three  $s$  quarks in the  $\Omega^-$  therefore *cannot* be in the same state. So how do they differ?

The  $\Omega^-$  is an obvious example of the contradiction, but it turns out that in order for the predictions of the quark model to agree with the observed spectrum of hadron multiplets, it is necessary to assume that overall baryon wavefunctions are symmetric under the interchange of like quarks.<sup>2</sup> In order to resolve this contradiction, it is necessary to assume that a new degree of freedom exists for quarks, but not leptons, which is somewhat whimsically called *colour*. The basic properties of colour are as follows.

1. Any quark  $u, d, s, \dots$  can exist in three different colour states.<sup>3</sup> We shall see later that there is direct experimental evidence that just three such states exist, which we denote  $r, g, b$  for ‘red’, ‘green’ and ‘blue’ respectively.
2. Each of these states is characterized by the values of two conserved *colour charges*, denoted  $I_3^C$  and  $Y^C$ , which are strong interaction analogues of the electric charge in electromagnetic interactions.<sup>4</sup> These charges depend only on the colour states  $r, g, b$  and *not* on the flavours  $u, d, s, \dots$ . The particular values for quarks and antiquarks are given in Table 5.1, and are a consequence of a fundamental symmetry of the strong interaction (called SU(3) colour symmetry), which we will not pursue here. For multiparticle states, the colour charges of the individual states are simply added.
3. Only states with zero values for the colour charges are observable as free particles; these are called *colour singlets*. This is the hypothesis of *colour confinement*. It can be derived, at least approximately, from the theory of strong interactions we shall describe.

**Table 5.1** Values of the colour charges  $I_3^C$  and  $Y^C$  for the colour states of quarks and antiquarks

	(a) Quarks		(b) Antiquarks		
	$I_3^C$	$Y^C$	$I_3^C$	$Y^C$	
$r$	$\frac{1}{2}$	$\frac{1}{3}$	$\bar{r}$	$-\frac{1}{2}$	$-\frac{1}{3}$
$g$	$-\frac{1}{2}$	$\frac{1}{3}$	$\bar{g}$	$\frac{1}{2}$	$-\frac{1}{3}$
$b$	0	$-\frac{2}{3}$	$\bar{b}$	0	$\frac{2}{3}$

<sup>2</sup>In Problem 3.4 it was shown explicitly that otherwise the wrong hadron spectrum is predicted.

<sup>3</sup>Needless to say, nothing to do with ‘real’ colour!

<sup>4</sup>This is one reason we were careful to use the qualifier ‘electric’ when talking about charge in the context of electromagnetic interactions in earlier chapters.

Returning to the quark model, it can be seen from Table 5.1 that a  $3q$  state can only have both  $I_3^C = 0$  and  $Y^C = 0$  if we have one quark in an  $r$  state, one in a  $g$  state and one in a  $b$  state. Hence in the  $\Omega^-$ , for example, all three  $s$  quarks are necessarily in different colour states, and thus the Pauli principle can be satisfied. Formally, we are assuming that the total wavefunction is the product of a spatial part  $\psi_{\text{spatial}}(\mathbf{x})$  and a spin part  $\psi_{\text{spin}}$ , as usual, but also a colour wavefunction  $\psi_{\text{colour}}$ , i.e.

$$\Psi = \psi_{\text{spatial}}(\mathbf{x}) \psi_{\text{spin}} \psi_{\text{colour}}. \quad (5.1)$$

The Pauli principle is now interpreted as applying to the total wavefunction including the colour part  $\psi_{\text{colour}}$ . The combined space and spin wavefunctions can then be symmetric under the interchange of quarks of the same flavour (to agree with experiment) provided the colour wavefunction is antisymmetric. The structure of  $\psi_{\text{colour}}$  is

$$\psi_{\text{colour}} = \frac{1}{\sqrt{6}} [R_1 G_2 B_3 + G_1 B_2 R_3 + B_1 R_2 G_3 - R_1 B_2 G_3 - B_1 G_2 R_3 - G_1 R_2 B_3], \quad (5.2)$$

where  $R$ ,  $G$  and  $B$  represent quarks with colour red, green and blue, respectively.

One can also see from Table 5.1 part of the answer to the first question of this section. Free quarks and fractionally charged combinations like  $qq$  and  $qq\bar{q}$  are forbidden by colour confinement, in accordance with experimental observation. On the other hand, the combinations  $q\bar{q}$  and  $3q$  used in the simple quark model are allowed. More unusual combinations like  $qq\bar{q}\bar{q}$  and  $qqqq\bar{q}$ , which could give rise to so-called ‘exotic’ mesons and baryons, respectively, are not in principle forbidden by colour confinement and, as mentioned in Chapter 3, recent experiments may possibly have provided some evidence for a small number of these, but this has yet to be confirmed.

## 5.2 Quantum Chromodynamics (QCD)

The theory that describes strong interactions in the standard model is called *quantum chromodynamics*, or QCD for short (chromos means colour in Greek). Although QCD is not tested to the same extent or precision as quantum electrodynamics (QED), the quantum theory of electromagnetic interactions, it is nevertheless in impressive agreement with a large body of experimental data. QCD is similar to QED in that both describe interactions that are mediated by massless spin-1 bosons; gluons in the former case and photons in the latter. Both theories are of the type called *gauge theories* which, as mentioned in Chapter 1, refer to a particular symmetry of the theory. However, there is a very important difference in the two interactions that we now discuss.

Gluons, the force carriers of the strong interaction, have zero electric charge, like photons, but unlike photons, which couple to electric charge, gluons couple to *colour* charges. This leads immediately to the flavour independence of strong interactions discussed in Chapter 3; that is, the different quark flavours  $a = u, d, s, c, b$  and  $t$  have identical strong interactions. We now see that this is because they are postulated to exist in the same three colour states  $r, g, b$ , with the same possible values of the colour charges. Flavour independence has its most striking consequences for  $u$  and  $d$  quarks, which have almost equal masses, where it leads to the phenomenon of isospin symmetry. This results, among other things, in the near equality of the masses of the proton and neutron, and charge states within other multiplets such as pions and kaons, all of which we have seen in Chapter 3 are confirmed by experiment. We will examine the consequence of flavour independence for the bound states of the heavy quarks  $c$  and  $b$  in Section 5.3.

Although QED and QCD both describe interactions, albeit of very different strengths, that are mediated by massless spin-1 bosons which couple to conserved charges, there is a crucial difference between them that profoundly effects the characters of the resulting forces. While the photons which couple to the electric charge are themselves electrically neutral, gluons have non-zero values of the colour charges to which they couple. This is illustrated in Figure 5.1, which shows a particular example of a quark–quark interaction by gluon exchange.

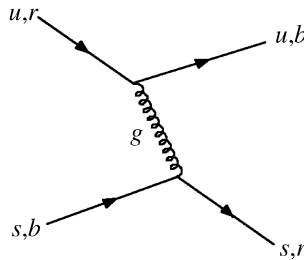


**Figure 5.1** Example of quark–quark scattering by gluon exchange; in this diagram, the quark flavours  $u$  and  $s$  are unchanged, but their colour states can change, as shown

In this diagram, the colour states of the two quarks are interchanged, and the gluon has non-zero values of the colour quantum numbers, whose values follow from colour charge conservation at the vertices, i.e.

$$I_3^C(g) = I_3^C(r) - I_3^C(b) = \frac{1}{2} \quad (5.3)$$

and

$$Y^C(g) = Y^C(r) - Y^C(b) = 1. \quad (5.4)$$

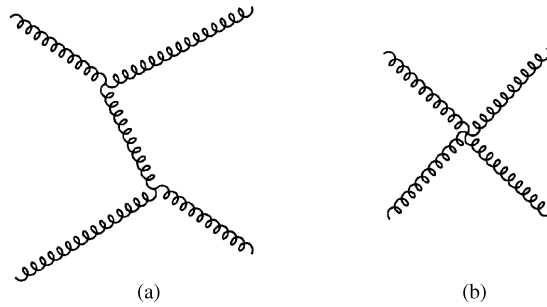


**Figure 5.2** The two lowest-order contributions to gluon-gluon scattering in QCD: (a) one-gluon exchange, (b) contact interaction

Just as quarks can exist in three colour states, gluons can exist in eight colour states, although we will not need the details of these. The first thing implied by the non-zero values of the colour charges is that gluons, like quarks, are confined and cannot be observed as free particles. The second is that since gluons couple to particles with non-zero colour charges, and since gluons themselves have non-zero colour charges, it follows that gluons couple to other gluons. The two types of gluon self-coupling that occur in QCD are given in Figure 5.2, which shows the two lowest-order contributions to gluon-gluon scattering.

The first is a gluon exchange process in analogy to gluon exchange in quark-quark scattering, which we have encountered previously (see Figure 1.3), while the second involves a so-called ‘zero range’ or ‘contact’ interaction. If the forces resulting from these interactions were attractive and sufficiently strong, they could in principle lead to bound states of two or more gluons. These would be a new type of exotic state called *glueballs*. Although some experiments claimed to have detected these, at present there is little compelling evidence that they exist.<sup>5</sup>

The gluon-gluon interactions have no analogue in QED (photons couple to electrically charged particles and hence do not couple directly to other photons) and it can be shown that they lead to properties of the strong interaction that differ markedly from those of the electromagnetic interaction. These properties are *colour confinement*, which we have discussed above, and a new property called *asymptotic freedom*. The latter is the statement that the strong interaction gets weaker at short distances; conversely, as the distance between the quarks increases, the interaction gets stronger.<sup>6</sup> In this strong interaction regime the situation is very complicated, and it has not yet been possible to evaluate the theory precisely. We therefore have to rely on results obtained by numerical simulations of the theory; the approach is called *lattice gauge theory*. In these simulations, the theory is

<sup>5</sup>A critical review is given in Ei04.

<sup>6</sup>Asymptotic freedom was postulated in 1973 by David Gross, David Politzer and Frank Wilczek, who were subsequently awarded the 2004 Nobel Prize in Physics.

evaluated at a grid of discrete points on a three-dimensional lattice and by making the lattice spacing small enough it is hoped that the results of the true continuum theory will be approximated. The calculations require very large ultra-fast computers and precise results are difficult to obtain because of the approximations that have to be made. Nevertheless, at present, the demonstration of confinement in QCD rests largely on such simulations.<sup>7</sup>

### 5.3 Heavy Quark Bound States

Some of the features of QCD discussed above are illustrated by considering the static potential between a heavy quark and an antiquark. Such systems give rise to bound states and because the quarks are so heavy they move slowly enough within the resulting hadrons to be treated non-relativistically to a first approximation. (This is one of the few places in particle physics where a non-relativistic calculation is adequate.) This means that the rest energies of the bound states, and hence their masses, can be calculated from the static potential between the quarks in exactly the same way that the energy levels in the hydrogen atom are calculated, although of course the potential is not Coulombic. In the present case, however, the procedure is reversed, with the aim of determining the form of the static potential from the rather precisely measured energies of the bound states.

The first such state to be discovered, the  $J/\psi(3097)$ <sup>8</sup>, is a bound state of the  $c\bar{c}$  system and is part of a family of such states given the name *charmonium*, by analogy with *positronium*, the bound state of an electron and a positron. It is identified with the  $n = 1$ ,  $^3S_1$  state of the  $c\bar{c}$  system, where  $n$  is the principal quantum number and we use the notation  $^{2S+1}L_J$ , with  $(L, S)$  the angular momentum between the quarks and their total spin, respectively. The discovery of the  $J/\psi(3097)$  caused considerable excitement because it confirmed the existence of the charm quantum number that had been predicted many years earlier, even though the  $J/\psi(3097)$  itself has zero overall charm. It was hence a very important piece of evidence in favour of the standard model.

The interpretation of the  $J/\psi(3097)$  as a  $c\bar{c}$  bound state follows from its unusually narrow width. For a state decaying predominantly (86 per cent) to hadrons (mostly pions) by the strong interaction one would expect a width measured in MeV, whereas the width of the  $J/\psi(3097)$  was only about 90 keV. This meant that there was no possibility of an explanation in terms of just  $u$ ,  $d$  and  $s$  quarks. The preferred decay of the  $J/\psi(3097)$  would be via the mechanism shown in Figure 5.3(a). However, this is forbidden by energy conservation because

<sup>7</sup>Lattice calculations also support the view that gluon–gluon forces are strong enough to give rise to glueballs.

<sup>8</sup>The rather clumsy notation is because it was discovered independently by two groups, led by Burton Richer and Samuel Ting. Richer's group was studying the reactions  $e^+e^- \rightarrow$  hadrons and named it the  $\psi$  particle. Ting's group discovered it in  $p$ Be reactions and called it the  $J$ . It is now known as the  $J/\psi$ . Richer and Ting shared the 1976 Nobel Prize in Physics for the discovery.

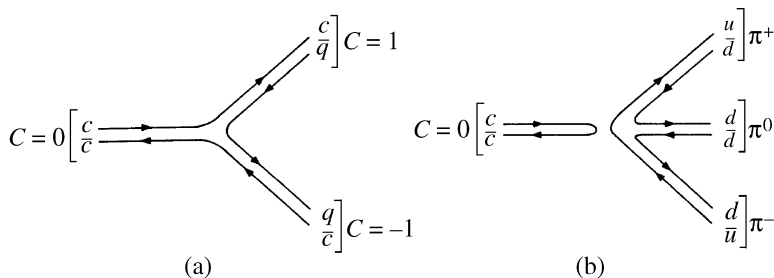


**Figure 5.3** Quark diagrams for (a) the decay of a charmonium state to a pair of charmed mesons, and (b) an example of a decay to non-charmed mesons

$M_{J/\psi} < 2M_D$ , where  $M_D$  is the mass of the lightest meson having non-zero charm, the  $D(1870)$ . (These latter states had already been seen in neutrino experiments, but not clearly identified.) The mass  $2M_D$  is referred to as the *charm threshold*. Since the direct decay to charmed mesons is forbidden, the only hadronic decays allowed must proceed via mechanisms such as that of Figure 5.3(b) and diagrams like this where initial and final quark lines are disconnected are known to be heavily suppressed.<sup>9</sup>

The explanation for this in QCD is that since both the decaying particle and the three pions in the final state are colour singlets, they can only be connected by the exchange of a combination of gluons that is also a colour singlet, i.e. not the exchange of a single gluon. Moreover, the  $J/\psi(3097)$  is known to be produced in  $e^+e^-$  annihilations via photon exchange, so it must have a charge conjugation  $C = -1$ . Thus the minimum number of gluons exchanged is three. This is illustrated in Figure 5.4. In contrast, if  $M_\psi > 2M_D$  then the decay may proceed via the exchange of low-momentum gluons as usual.

Subsequently, higher-mass charmonium states also with  $J^{PC} = 1^{--}$ , where  $P = (-1)^{L+1}$  and  $C = (-1)^{L+S}$ , were discovered in  $e^+e^-$  reactions and states with other  $J^{PC}$  values were identified in their radiative decays. Thus the  $n = 1, {}^1S_0$

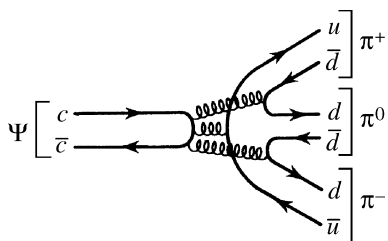


**Figure 5.4** OZI-suppressed decay of a charmonium state below the  $D\bar{D}$  threshold

<sup>9</sup>This is known as the *OZI Rule* after Okubo, Zweig and Iizuka who first formulated it. Another example where it acts is the suppression of the decay  $\phi \rightarrow \pi^+\pi^-\pi^0$  compared with  $\phi \rightarrow K\bar{K}$ .

ground state  $\eta_c(2980)$  has been found from the decays

$$\psi(3686) \rightarrow \eta_c(2980) + \gamma \quad \text{and} \quad J/\psi(3097) \rightarrow \eta_c(2980) + \gamma \quad (5.5)$$

and a series of states  $\chi_{ci}(i = 1, 3)$  have been found in the decays

$$\psi(3686) \rightarrow \chi_{ci} + \gamma. \quad (5.6)$$

The latter themselves decay and from an analysis of their decay products they are identified with the  $n = 1$  states  $^3P_0$ ,  $^3P_1$  and  $^3P_2$ . Some of these states lie below the charm threshold and like the  $J/\psi(3097)$  are forbidden by energy conservation to decay to final states with ‘open’ charm and thus have widths measured in keV. Others lie above the charm threshold and therefore have ‘normal’ widths measure in MeV. The present experimental situation for charmonium states with  $L \leq 2$  is shown in Table 5.2.

**Table 5.2** Predicted  $c\bar{c}$  and  $b\bar{b}$  states with  $L \leq 2$  and masses up to and just above the charm and bottom thresholds ( $3.74 \text{ GeV}/c^2$  and  $10.56 \text{ GeV}/c^2$ , respectively), compared with experimentally observed states (masses are given in  $\text{MeV}/c^2$ )

$n^{2S+1}L_J$	$J^{PC}$	$c\bar{c}$ state	$b\bar{b}$ state
$1^1S_0$	$0^{-+}$	$\eta_c(2980)$	$\eta_b(9300)?$
$1^3S_1$	$1^{--}$	$J/\psi(3097)$	$\Upsilon(9460)$
$1^1P_1$	$1^{+-}$	$h_c(3526)?$	
$1^3P_0$	$0^{++}$	$\chi_{c0}(3415)$	$\chi_{b0}(9860)$
$1^3P_1$	$1^{++}$	$\chi_{c1}(3511)$	$\chi_{b1}(9893)$
$1^3P_2$	$2^{++}$	$\chi_{c2}(3556)$	$\chi_{b2}(9913)$
$2^1S_0$	$0^{-+}$	$\eta_c(3654)?$	
$2^3S_1$	$1^{--}$	$\psi(3686)$	$\Upsilon(10023)$
$2^3P_0$	$0^{++}$		$\chi_{b0}(10232)$
$2^3P_1$	$1^{++}$		$\chi_{b1}(10255)$
$2^3P_2$	$2^{++}$		$\chi_{b3}(10269)$
$3^3S_1$	$1^{--}$	$\psi(4040)$	$\Upsilon(10355)$
$4^3S_1$	$1^{--}$	$\psi(4160)$	$\Upsilon(10580)$

Later experiments established a spectrum of *bottomium* states, i.e. bound states of the  $b\bar{b}$  system. These are also shown in Table 5.2. By analogy with charmonium, those bottomium states below the *bottom threshold*  $2M_B = 10.56 \text{ GeV}/c^2$ , where  $M_B$  is the mass of the lightest meson with non-zero beauty quantum number, have widths measured in keV, whereas those above this threshold have ‘normal’ widths expected of resonances decaying via the strong interaction

The charmonium and bottomium states with  $L \leq 2$  are shown in Figure 5.5 as conventional energy level diagrams, where the energies are plotted relative to those

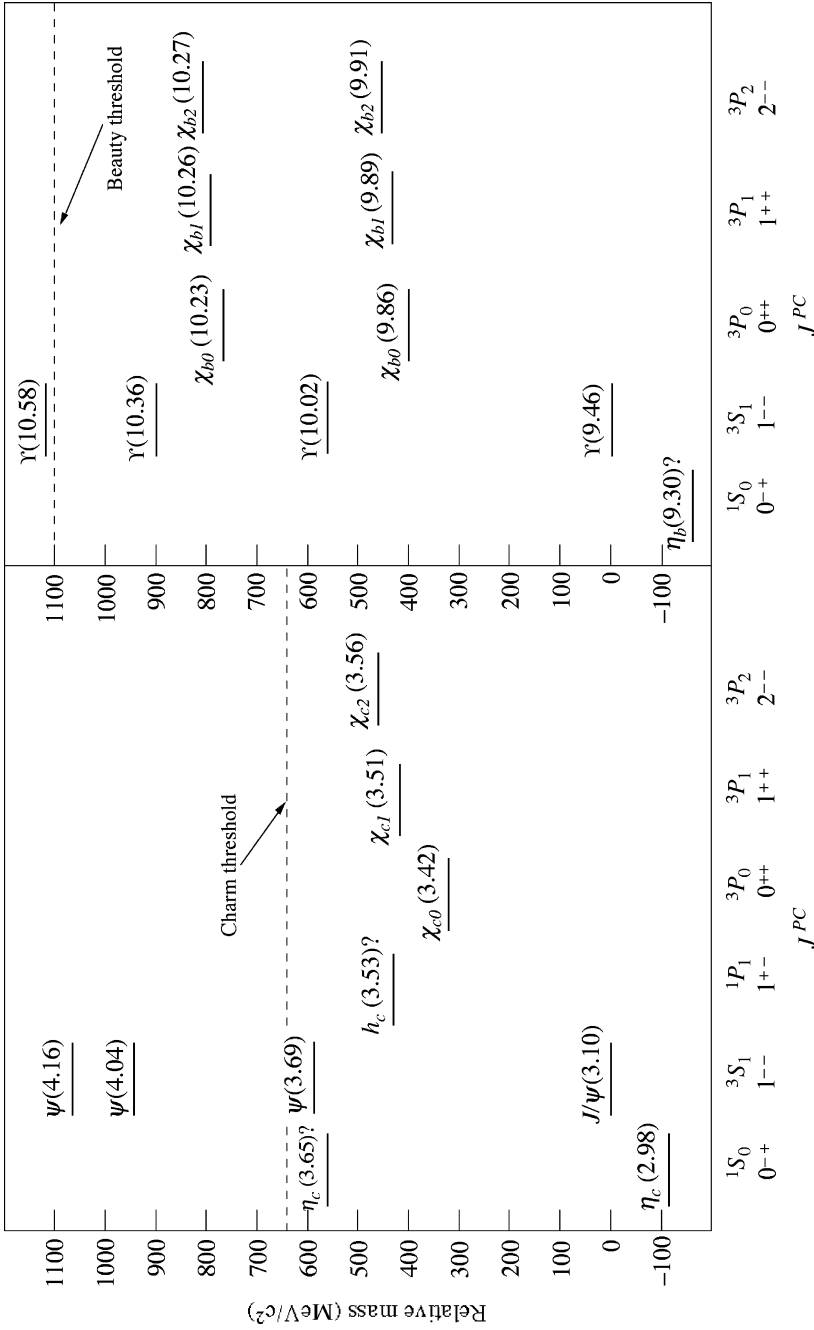


**Figure 5.5** Energy levels of the charmonium ( $cc$ ) and bottomonium ( $bb$ ) states for  $L \leq 2$ ; the masses are given in units of  $\text{GeV}/c^2$

of the  ${}^3S_1$  ground states. There is a striking similarity in the levels of the two systems, which suggests that the forces in the  $c\bar{c}$  and  $b\bar{b}$  are flavour independent, as discussed in Chapter 3 and now seen to follow from the postulates of QCD. The level structure is also very similar to that seen in positronium which suggests that, as in positronium, there is a major contribution from a single-particle exchange with the Coulomb-like form. In fact at short interquark distances  $r \lesssim 0.1$  fm, the interaction is dominated by one-gluon exchange that we can write as

$$V(r) = -\frac{a}{r}, \quad (5.7)$$

where  $a$  is proportional to the strong interaction analogue of the fine structure constant  $\alpha$  in QED. Because of asymptotic freedom, the strength of the interaction decreases with decreasing  $r$ , but for  $r < 0.1$  fm this variation is slight and can in many applications be neglected.<sup>10</sup>

In strong interactions we also have to take account of the fact that the quarks are confined. The latter part of the potential cannot at present be calculated from QCD and several forms are used in phenomenological applications. All reasonable forms are found to give very similar results for the region of interest. If we choose a linear form, then

$$V(r) \approx b r. \quad (5.8)$$

This is an example of a *confining potential*, in that it does not die away with increasing separation and the force between the quark and antiquark cannot be neglected, even when they are very far apart. The full potential is thus

$$V(r) = -\frac{a}{r} + br. \quad (5.9)$$

If the form (5.9) is used in the Schrödinger equation for the  $c\bar{c}$  and  $b\bar{b}$  systems, taking account of their different masses, it is found that a good fit to both sets of energy levels can be obtained for the *same* values  $a \approx 0.48$  and  $b \approx 0.18 \text{ GeV}^2$ , which confirms the flavour independence of the strong interaction and is evidence for QCD and the standard model.

## 5.4 The Strong Coupling Constant and Asymptotic Freedom

The strong interaction derives its name from the force that, among other things, binds quarks into hadrons. However, some remarkable phenomena depend on the fact that the interaction gets weaker at short distances; that is, on asymptotic

---

<sup>10</sup>The equivalent coupling in QED also varies with distance, but the variation is very small and can usually be neglected.

freedom. Such short-distance interactions are associated with large momentum transfers  $|\mathbf{q}|$  between the particles, with  $|\mathbf{q}| = O(\hbar/r)$ , where  $r$  is the distance at which the interaction occurs. Hence in discussing scattering from a static potential, like the one above, we can regard the strong coupling  $\alpha_s$  as decreasing with increasing momentum transfer, rather than with decreasing  $r$ .

In general, the strength of the interaction can be shown to depend on the squared four-momentum transfer

$$Q^2 \equiv E_q^2/c^2 - \mathbf{q}^2, \quad (5.10)$$

which was introduced in Chapter 2. Specifically, it can be shown that the QCD coupling constant  $\alpha_s$  is given to a good approximation by

$$\alpha_s = \frac{12\pi}{(33 - 2N_f) \ln(Q^2/\Lambda^2)}, \quad (5.11)$$

where  $N_f$  is the number of quark flavours  $u, d, s, \dots$ , with  $4m_q^2c^4 < Q^2$ , and  $Q^2 \gg \Lambda^2$ . The constant  $\Lambda$  is a scale parameter that must be determined from experiment. Thus QCD does not predict the absolute value of  $\alpha_s$ , but rather its dependence on  $Q^2$ . The value of  $\Lambda$  may be found by measuring the coupling constant in a variety of processes (two of which will be discussed later in this chapter) giving values consistent with

$$\Lambda = 0.2 \pm 0.1 \text{ GeV}/c. \quad (5.12)$$

Because  $\alpha_s$  varies with  $Q^2$ , it is often referred to as the *running coupling constant*. The values of  $\alpha_s(Q^2)$  corresponding to Equation (5.12) are plotted in Figure 5.6. The

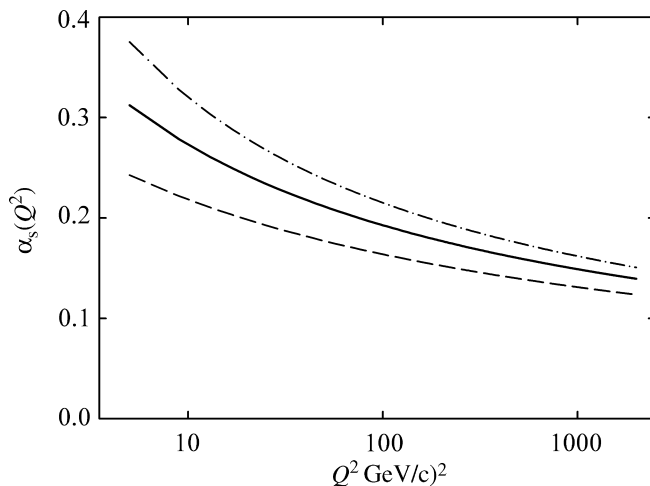


**Figure 5.6** The running coupling constant  $\alpha_s$  corresponding to four flavours and a scale parameter  $\Lambda = 0.2 \pm 0.1 \text{ GeV}/c$ ; the dashed, solid and dot-dashed curves correspond to  $\Lambda = 0.1, 0.2$  and  $0.3$ , respectively

variation with  $Q^2$  is small at large  $Q^2$  and over limited  $Q^2$  regions it can often be neglected. In this large  $Q^2$  region, the coupling is sufficiently weak that calculations can be performed with reasonable accuracy by retaining only diagrams of lowest and next-to-lowest order; and sometimes the short-range strong interaction can be neglected to a first approximation, as we shall see.

Although there are other forces that increase with increasing separation (for example, the force between two particles connected by a spring or elastic string), the difference between those and the present case is that in the former cases eventually something happens (for example, the string breaks) so that the particles (or the ends of the string) become free. This does not happen with the strong force. Instead, the energy stored in the colour field increases until it becomes sufficiently large to create  $q\bar{q}$  pairs and eventually combinations of these will appear as physical hadrons. This latter process is called *fragmentation* and is rather poorly understood. The behaviour of the strong interaction as a function of distance (or equivalently momentum transfer) is so unlike the behaviour of other forces we are familiar with (e.g. gravity and electromagnetism) that it is worth looking at why this is.

In QED, single electrons are considered to emit and reabsorb photons continually, as shown in Figure 5.7(a). Such a process is an example of a so-called *quantum fluctuation*, i.e. one particle converting to two or more particles for a finite time. This is allowed provided the time and the implied violation of energy conservation are compatible with the uncertainty principle. Of course if another electron is nearby, then it may absorb the photon and we have the usual one-photon exchange scattering process of Figure 5.7(b).

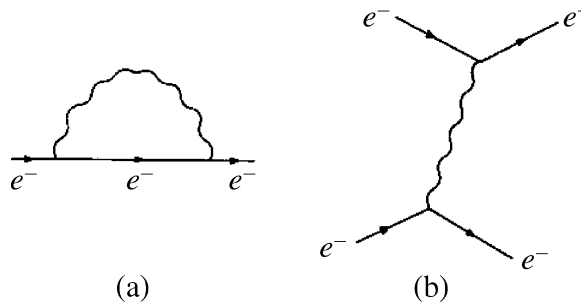


**Figure 5.7** (a) The simplest quantum fluctuation of an electron, and (b) the associated exchange process

The emitted photon may itself be subject to quantum fluctuations, leading to more complicated diagrams like those shown in Figure 5.8(a). Thus the initial electron emits not only photons, but also indirectly electron–positron pairs. These are referred to as a ‘sea’ of virtual electrons (cf. comments in Chapter 3 in the context of the quark model). The equivalent contribution to elastic electron–electron scattering is shown in Figure 5.8(b).

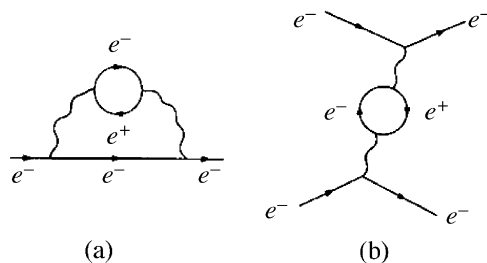


**Figure 5.8** (a) A more complicated quantum fluctuation of the electron, and (b) the associated exchange process

These virtual processes are collectively referred to as *vacuum polarization effects*.<sup>11</sup> The production of virtual  $e^+e^-$  pairs produces a shielding effect, so that the charge and the strength of the interaction  $\alpha$ , as seen from a distance, will appear altered. Detailed calculations show that if we write the Coulomb potential as

$$\phi_{\text{eff}}(r) = \frac{\alpha_{\text{eff}}(r)\hbar c}{r}, \quad (5.13)$$

then

$$\alpha_{\text{eff}} = \alpha \approx 1/137 \quad (5.14)$$

for

$$r \gg r_C \equiv \hbar/mc = 3.9 \times 10^{-13} \text{ m}, \quad (5.15)$$

but for  $r \leq r_C$ , the value of  $\alpha$  is somewhat larger and increases as  $r$  becomes smaller. In other words, the strength of the interaction increases at very short distances. Formally, without proof, the QED coupling  $\alpha_{\text{em}}(Q^2)$  is given by

$$\alpha_{\text{em}}(Q^2) = \alpha(\mu^2) \left[ 1 - \frac{1}{3\pi} \alpha(\mu^2) \ln\left(\frac{Q^2}{\mu^2}\right) \right]^{-1}, \quad (5.16)$$

where  $\mu^2$  is a low-energy value of  $Q^2$  at which the value of  $\alpha$  is known. If, for example, we take  $\mu = 1 \text{ MeV}/c$  and  $\alpha = 1/137$ , i.e. the value of the fine structure constant as found from low-energy interactions, then at the mass of the  $Z^0$  boson,  $\alpha \approx 1/135$ . Thus the electromagnetic coupling increases with energy-transfer, but only very slowly.

<sup>11</sup>The name arises from the analogy of placing a charge in a dielectric medium. This aligns the particles of the medium and produces a net polarization.

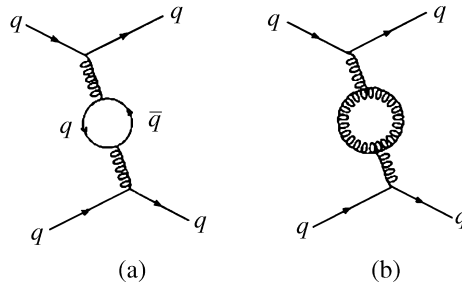


**Figure 5.9** The two lowest-order vacuum polarization corrections to one-gluon exchange in quark--quark scattering

Vacuum polarization effects have measurable consequences. For example, the 2S state in hydrogen is predicted to be more tightly bound than it would be in a pure Coulomb potential. The increased binding is only  $2.2 \times 10^{-7}$  eV, but nevertheless it is confirmed by extremely accurate measurements on the hydrogen spectrum. There are also very small corrections to the magnetic moment of the electron that have been verified experimentally to extraordinary precision.

Quantum fluctuations also exist in QCD and also give rise to a variation of the interaction strength with distance. If, by analogy with QED, we consider quark--quark scattering, then the two lowest-order vacuum polarization corrections are shown in Figure 5.9. The first of these (Figure 5.9(a)) is analogous to virtual  $e^+e^-$  production in QED and also leads to a screening effect. However, the second diagram (Figure 5.9(b)) has no counterpart in QED, because there are no direct photon self-couplings. Calculations show that this diagram leads to an *antiscreening* effect that is larger than the screening effect from Figure 5.9(a) and so the net effect is that the interaction grows *weaker* at short distances, i.e. asymptotic freedom. Formally, the strong interaction coupling  $\alpha_s$  is given by a formula analogous to that for  $\alpha_{em}$  above, except the coefficient of the logarithmic term is different and, crucially, its sign is positive:

$$\alpha_s(Q^2) = \alpha_s(\mu^2) \left[ 1 + \frac{\alpha_s(\mu^2)}{12\pi} (33 - 2N_f) \ln(Q^2/\mu^2) \right]^{-1}, \quad (5.17)$$

where again  $\mu^2$  is a low-energy value of  $Q^2$  at which the value of  $\alpha_s$  is known and  $N_f$  is the number of quark flavours that take part in the interaction.

## 5.5 Jets and Gluons

A striking feature of many high-energy particle collisions is the occurrence of jets of hadrons in the final state. We have already mentioned these in Section 3.2.1 when we discussed the experimental evidence for quarks and again when we

discussed basic properties of quarks and gluons interactions earlier in this chapter. They have been extensively studied in the reaction

$$e^+ + e^- \rightarrow \text{hadrons} \tag{5.18}$$

at high energies using colliding beam experiments, which were discussed in Chapter 4. High-energy electrons and positrons collide head-on, with equal and opposite momenta, so that the total momentum of the hadrons produced cancels out to zero in order to conserve momentum. This is a particularly ‘clean’ reaction, because the initial particles are elementary, without internal structure.

In the centre-of-mass energy range 15–40 GeV, electron–positron annihilation into hadrons is dominated by the production of jets. These can be regarded as occurring in two stages: (1) a primary electromagnetic process  $e^+ + e^- \rightarrow q + \bar{q}$  (due to photon exchange) leading to the production of a quark–antiquark pair, followed by (2) fragmentation (the concept we met in discussing asymptotic freedom) which converts the high-energy  $q\bar{q}$  pair into two jets of hadrons. This is illustrated in Figure 5.10.

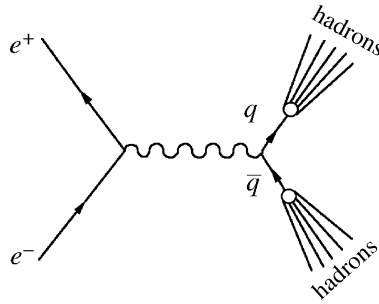


**Figure 5.10** Basic mechanism of two-jet production in electron–positron annihilation

The fragmentation process that converts the quarks into hadrons is very complicated, and the composition of the jets – i.e. the numbers and types of particles in the jet and their momenta – varies from event to event. However, the direction of a jet, defined by the total momentum vector

$$\mathbf{P} = \sum_i \mathbf{p}_i, \tag{5.19}$$

where the sum extends over all the particles within the jet, closely reflects the parent quark or antiquark direction. This is because the QCD interaction is relatively weak at very short distances (asymptotic freedom), and the quark and antiquark do not interact strongly until they are separated by a distance  $r$  of order 1 fm. At these relatively large distances, only comparatively small momenta can be transferred, and hence the jets that subsequently develop point almost exactly in the initial quark and antiquark directions. That is, the jet angular distribution relative to the electron beam direction reflects the angular distributions of the quark and antiquark in the basic reaction  $e^+ + e^- \rightarrow q + \bar{q}$ . The latter can easily

be calculated in QED as it is a purely electromagnetic process, and is in excellent agreement with the observed angular distribution of the jets. This is one of the pieces of evidence for the existence of quarks that was cited in Chapter 3 and again at the start of the present chapter.

Although the dominant process in electron–positron annihilation into hadrons is the formation of two ‘back-to-back’ jets, occasionally we would expect a high-momentum gluon to be emitted by the quark or anti-quark before fragmentation occurs, in much the same way as a high-energy electron sometimes emits a photon (i.e. bremsstrahlung). The quark, antiquark and gluon then all fragment into hadrons, leading to a three-jet event. A computer reconstruction of such an event in a jet chamber is shown in Figure 5.11.

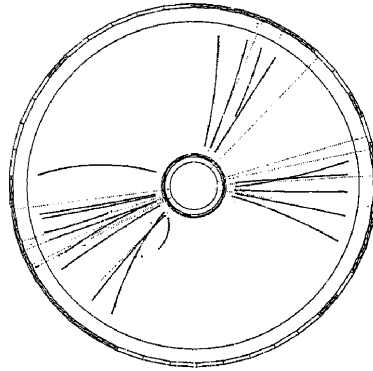


**Figure 5.11** Computer reconstruction of a three-jet event in electron–positron annihilation

Events like these provided the first unambiguous evidence for gluons, because the angular distributions of the jets are found to be in good agreement with the theoretical expectation for spin-1 gluons, but are inconsistent with what would be expected if, for example, the third jet originated from a particle of spin-0. The ratio of three-jet to two-jet events can also be calculated, assuming that the third jet is a gluon, because the probability that a quark or antiquark will emit a gluon is determined by the strong coupling  $\alpha_s$ , in the same way that the probability that an electron or positron will emit a photon is determined by the fine structure constant  $\alpha$ . This leads to a value of  $\alpha_s$  and hence  $\Lambda$ , the QCD scale parameter. The value obtained is consistent with Equation (5.12) found from other determinations and lends further support for the whole picture of quarks interacting via the exchange of gluons.

## 5.6 Colour Counting

What evidence is there that quarks exist in just three colour states? This question can be settled by using data from electron–positron annihilation. The cross-sections for

electron–positron annihilation to hadrons and for electron–positron annihilation to muons<sup>12</sup> both decrease rapidly with energy, but their ratio

$$R \equiv \frac{\sigma(e^+e^- \rightarrow \text{hadrons})}{\sigma(e^+e^- \rightarrow \mu^+\mu^-)} \quad (5.20)$$

is almost energy independent. The near constancy of this ratio follows from the dominance of the two-step mechanism of Figure 5.10, with the total annihilation rate being determined by that of the initial reaction  $e^+e^- \rightarrow q + \bar{q}$ . The value of the ratio  $R$  then directly confirms the existence of three colour states, each with the same electric charge, for each quark flavour.

To understand this, let us suppose that each quark flavour  $f = u, d, s, \dots$  exists in  $N_C$  colour states, so that  $N_C = 3$  according to QCD, while  $N_C = 1$  if the colour degree of freedom does not exist. Since the different colour states all have the same electric charge, they will all be produced equally readily by the mechanism of Figure 5.10, and the rate for producing quark pairs of any given flavour  $f = u, d, s, \dots$  will be proportional to the number of colours  $N_C$ . The cross-section is also proportional to the squared charge of the produced pair (because this is a first-order electromagnetic process), and since muon pairs are produced by an identical mechanism, we obtain

$$\sigma(e^+e^- \rightarrow q\bar{q}) = N_C e_f^2 \sigma(e^+e^- \rightarrow \mu^+\mu^-), \quad (5.21)$$

where  $e_f$  is the electric charge, in units of  $e$ , on a quark of flavour  $f$ .

The cross-section for  $e^+ + e^- \rightarrow \text{hadrons}$  will receive an additional contribution of the form of Equation (5.21) when the energy passes a threshold for a new quark flavour to be produced. Thus  $R$  at low energies will have a series of ‘steps’ corresponding to the production of pairs of new quarks and this is what is observed experimentally. At high energies above the threshold for the production of  $b\bar{b}$  pairs and assuming that hadron production is completely dominated by the two-step process of Figure 5.10, we would have<sup>13</sup>

$$R = R_0 \equiv N_C(e_u^2 + e_d^2 + e_s^2 + e_c^2 + e_b^2) = 11N_C/9. \quad (5.22)$$

When the small contribution from the three-jet events and other corrections of order  $\alpha_s$  are taken into account, this expression for  $R$  is modified to

$$R = R_0(1 + \alpha_s/\pi), \quad (5.23)$$

<sup>12</sup>The cross-section for the production of muon pairs is essentially a purely electromagnetic one, except at very high energies where the effect of the weak interaction may be seen. This will be discussed in Chapter 6.

<sup>13</sup>There is no contribution from the top quark because it is too heavy to be produced, even at the high energies we are considering.

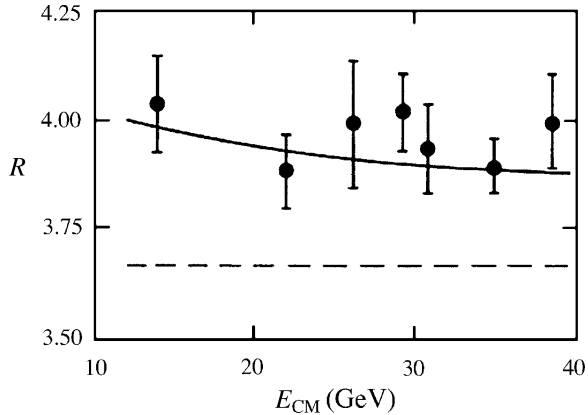


**Figure 5.12** Measured values of the cross-section ratio  $R$  and the theoretical prediction from QCD for  $N_C = 3$  colours; the dashed line shows the prediction without QCD corrections

giving rise to a weak energy dependence of  $R$  from the energy dependence of  $\alpha_s$  discussed earlier (Equation (5.17)). Although these corrections of order  $\alpha_s$  are small compared to the dominant contribution, they must be included if the most precise experimental data on  $R$  are to be accounted for. The data are in excellent agreement with the theoretical prediction for the value  $N_C = 3$  (see Figure 5.12) and hence prove that quarks exist in just three colour states.

## 5.7 Deep Inelastic Scattering and Nucleon Structure

In Chapter 2 we discussed the scattering of electrons from nuclei to determine their radial charge distributions. This was done by assuming a form for the charge distribution, calculating the resulting form factor (i.e. the Fourier transform of the charge distribution) and using it to fit experimental cross-sections. In a somewhat similar way we can use high-energy inelastic scattering to investigate the charge distribution within nucleons. This is referred to as *deep inelastic scattering*, because the projectiles probe deep into the internal structure of the nucleon. This type of interaction was mentioned in Section 2.9 in the context of classifying nuclear reaction mechanisms. The original experiments of this type in particle physics were done in the 1960s and provided the first definitive evidence for the existence of quarks. We will deduce that nucleons have a sub-structure of point-like charged constituents.<sup>14</sup>

<sup>14</sup>The pioneering work on deep inelastic scattering done by Jerome Friedman, Henry Kendall and Richard Taylor resulted in their receiving the 1990 Nobel Prize in Physics.

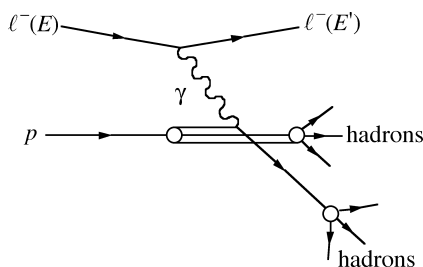


**Figure 5.13** Dominant one-photon exchange mechanism for inelastic lepton--proton scattering where  $\ell = e$  or  $\mu$

The dominant one-photon contribution to the inelastic scattering of a charged lepton from a proton in the spectator quark model is shown in Figure 5.13. Unlike elastic scattering, where at a given lepton energy  $E$  there is only one free variable (e.g. the scattering angle), in inelastic scattering the excitation energy of the nucleon adds a further degree of freedom, so we can define two independent variables. These are usually taken to be  $\nu$ , defined by

$$2M\nu \equiv W^2c^2 + Q^2 - M^2c^2 \quad (5.24)$$

and a dimensionless quantity (called the *scaling variable*) given by

$$x \equiv Q^2/2M\nu. \quad (5.25)$$

Here,  $M$  is the proton mass,  $W$  is the invariant mass of the final-state hadrons and  $Q^2$  is the squared energy-momentum transfer

$$Q^2 = (E - E')^2/c^2 - (\mathbf{p} - \mathbf{p}')^2. \quad (5.26)$$

The physical interpretation of  $x$  will be discussed below. In the rest frame of the initial proton,  $\nu$  reduces to

$$\nu = E - E' \quad (5.27)$$

and so is the Lorentz-invariant generalization for the energy transferred from the lepton to the proton.

In Chapter 2 we discussed several modifications to the formalism for describing the structure of nuclei obtained from scattering experiments. Here we are dealing with high-energy projectiles and so we will need to take all those corrections into account. In particular, the magnetic interaction introduces a second form factor. (cf Equation (2.14)). The two form factors, denoted  $W_1$  and  $W_2$ , are called *structure*

*functions* in this context. In terms of these, the differential cross-section may be written

$$\frac{d^2\sigma}{d\Omega dE'} = \left(\frac{d\sigma}{d\Omega}\right)_{\text{Mott}} [W_2(Q^2, \nu) + 2W_1(Q^2, \nu) \tan^2(\theta/2)], \quad (5.28)$$

where  $\theta$  is the lepton scattering angle. For values of  $W \leq 2.5 \text{ GeV}/c^2$ , the cross-sections show considerable structure due to the excitation of nucleon resonances, but above this mass they are smoothly varying. In the latter region, the values of the structure functions can be extracted from the data by choosing suitable parameterizations and fitting the available data in an analogous way to the way charge distributions of nuclei were deduced in Chapter 2.

Rather than  $W_1$  and  $W_2$ , it is usual to work with two related dimensionless structure functions defined by

$$F_1(x, Q^2) \equiv Mc^2 W_1(Q^2, \nu) \quad \text{and} \quad F_2(x, Q^2) \equiv \nu W_2(Q^2, \nu). \quad (5.29)$$

It is a remarkable fact that at fixed values of  $x$  the structure functions have only a very weak dependence on  $Q^2$ . This behaviour is referred to as *scaling* and is illustrated in Figure 5.14. As the Fourier transform of a spherically symmetric point-like distribution is a constant, we conclude that the proton has a sub-structure of point-like charge constituents.

The interpretation of scaling is simplest in a reference frame where the target nucleon is moving with a very high velocity, so that the transverse momenta and

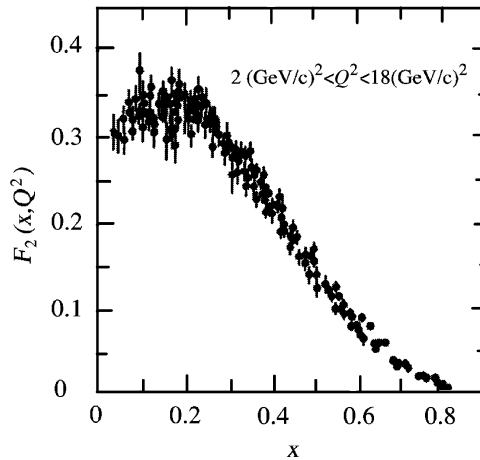


**Figure 5.14** The structure function  $F_2$  of the proton as a function of  $x$ , for  $Q^2$  between 2 and 18  $(\text{GeV}/c)^2$  (reproduced from At82 with kind permission of Springer Science and Business Media)

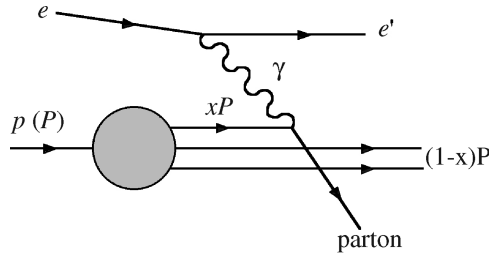


**Figure 5.15** The parton model of deep inelastic scattering

rest masses of its constituents may be neglected. The structure of the nucleon is then given by the longitudinal momentum of its constituents. This approach was first adopted by Feynman and Bjorken, who called the constituents *partons*. (We now identify charged partons with quarks and neutral partons with gluons.) In the *parton model*, deep inelastic scattering is visualized as shown in Figure 5.15. The target nucleon is a stream of partons each with four-momentum  $xP$ , where  $P = (p, \mathbf{p})$  is the four-momentum of the nucleon and  $p = |\mathbf{p}|$ , is its (very large) three-momentum, so that the nucleon mass may be neglected.

Suppose now that one parton of mass  $m$  is scattered elastically by the exchanged photon of four-momentum  $Q$ . Then

$$(xP + Q)^2 = (x^2P^2 + 2xP \cdot Q + Q^2) = m^2c^4 \approx 0. \quad (5.30)$$

If  $|x^2P^2| = x^2M^2c^4 \ll Q^2$ , then

$$x = -\frac{Q^2}{2P \cdot Q} = \frac{Q^2}{2M\nu}, \quad (5.31)$$

where the invariant scalar product has been evaluated in the laboratory frame in which the energy transfer is  $\nu$  and the nucleon is at rest. This is our previous definition Equation (5.25). Thus, the physical interpretation of  $x$  is the fractional three-momentum of the parton in the reference frame where the nucleon has a very high velocity. This is equivalent to having a parton of mass  $m$  stationary in the laboratory system, with the elastic relation  $Q^2 = 2m\nu$ . So provided  $Q^2 \gg M^2$ ,

$$x = \frac{Q^2}{2M\nu} = \frac{m}{M}, \quad (5.32)$$

i.e.  $x$  may also be interpreted as the fraction of the nucleon mass carried by the struck parton.

To identify the constituent partons with quarks we need to know their spins and charges. For the spin, it can be shown that

$$F_1(x, Q^2) = 0 \quad (\text{spin } 0) \quad (5.33)$$

and

$$2xF_1(x, Q^2) = F_2(x, Q^2) \quad (\text{spin } 1/2). \quad (5.34)$$

The latter relation, known as the *Callan–Gross relation*, follows by comparing the coefficients in the equation for the double differential cross-section Equation (5.28) with that in Chapter 2 (Equation (2.14)). This gives

$$2W_1/W_2 = 2\tau, \quad (5.35)$$

where  $\tau = Q^2/4m^2 c^2$  and  $m$  is the mass of the target, in this case the mass of the struck parton. Replacing  $W_1$  by  $F_1/Mc^2$  and  $W_2$  by  $F_2/\nu$ , gives

$$\frac{\nu}{Mc^2} \frac{F_1}{F_2} = \frac{Q^2}{4m^2 c^2} \quad (5.36)$$

and since now  $Q^2 = 2m\nu$ , we have  $m = Q^2/2\nu = xM$ . Finally, using this mass in Equation(5.36) yields the Callan–Gross relation. Figure 5.16 shows some results for the ratio  $2xF_1/F_2$ . It is clear that spin- $\frac{1}{2}$  is strongly favoured.

To deduce the parton charges is more complicated. We will assume that the constituent partons are quarks and show that this is consistent with experimental data. We start by defining  $q_f(x)$  to be the momentum distribution of a quark of flavour  $f$ , i.e.  $q_f(x)dx$  is the probability of finding in a nucleon a quark of flavour  $f$ , with momentum fraction in the interval  $x$  to  $x + dx$ . A given nucleon will consist of a combination of valence quarks (i.e. those that give rise to the observed quantum numbers in the quark model) and additional quark–antiquark pairs that are continually produced and annihilated by the radiation of virtual gluons by the quarks.<sup>15</sup> (Recall the discussion of quantum fluctuations in electrodynamics in Section 5.4.) Thus, in general, a structure function can be written as the sum of contributions from quarks and antiquarks of all flavours. Also, from the cross-section formula Equation (5.28), we would expect the structure functions to involve the quark distributions weighted by the squares of the quark charges  $z_f$  (in units of  $e$ ) for a given quark flavour  $f$ .

<sup>15</sup>These are the ‘sea’ quarks referred to in the discussion of the static quark model in Chapter 3.

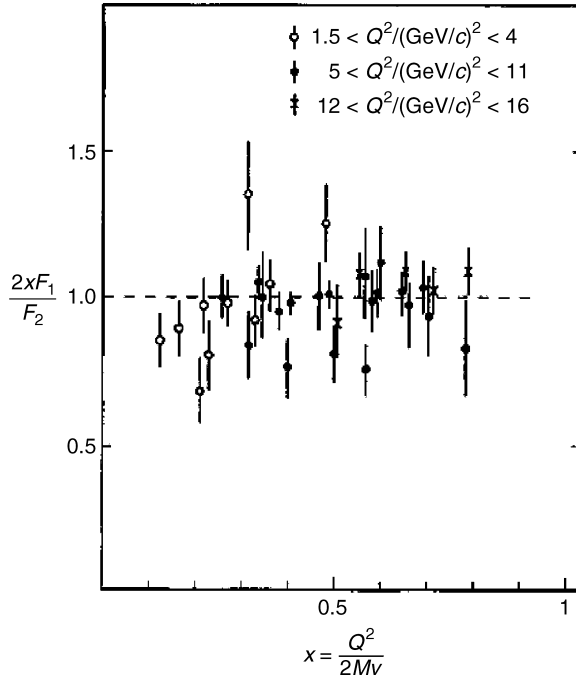


**Figure 5.16** The ratio  $2xF_1/F_2$  at fixed  $x$

Thus, for example,  $F_2$  is

$$F_2(x) = x \sum_f z_f^2 [q_f(x) + \bar{q}_f(x)]. \quad (5.37)$$

If we concentrate on the scattering of charged leptons, i.e. electrons or muons, and consider just the possibility of light quarks  $u$ ,  $d$  and  $s$  within nucleons, then we have (for  $\ell = e, \mu$ )

$$F_2^{\ell p}(x) = x \left[ \frac{1}{9}(d^p + \bar{d}^p) + \frac{4}{9}(u^p + \bar{u}^p) + \frac{1}{9}(s^p + \bar{s}^p) \right] \quad (5.38a)$$

and

$$F_2^{\ell n}(x) = x \left[ \frac{1}{9}(d^n + \bar{d}^n) + \frac{4}{9}(u^n + \bar{u}^n) + \frac{1}{9}(s^n + \bar{s}^n) \right], \quad (5.38b)$$

where, for example,  $u^{n,p}$  is the distribution of  $u$  quarks in the neutron and proton. Using isospin symmetry, interchanging  $u$  and  $d$  quarks changes neutron to proton,

i.e.  $u \leftrightarrow d$  implies  $n \leftrightarrow p$ . Thus,

$$u^p(x) = d^n(x) \equiv u(x), \quad (5.39a)$$

$$d^p(x) = u^n(x) \equiv d(x), \quad (5.39b)$$

and

$$s^p(x) = s^n(x) \equiv s(x), \quad (5.39c)$$

with similar relations for the antiquarks. Then if we work with a target nucleus with equal numbers of protons and neutrons (an *isoscalar* target), its structure function will have the approximate form (neglecting purely nuclear effects)

$$F_2^{\ell N}(x) = \frac{1}{2} [F_2^{\ell p}(x) + F_2^{\ell n}(x)] = \frac{5}{18} x \sum_{q=d,u} [q(x) + \bar{q}(x)] + \frac{1}{9} x [s(x) + \bar{s}(x)]. \quad (5.40)$$

The second term is small because  $s$  quarks are only present in the sea component at the level of a few percent. Thus the mean squared value of the charges of the  $u$  and  $d$  quarks is approximately  $\frac{5}{18}$ .

The final step is to extract information from deep inelastic scattering using neutrinos and antineutrinos as projectiles. This is more complicated because, as we shall see in Chapter 6, neutrinos and antineutrinos couple differently to the different quarks and antiquarks and there is also a third form factor involved. Without proof, we shall just quote the result:

$$F_2^{\nu N}(x) = x \sum_{q=d,u} [q(x) + \bar{q}(x)]. \quad (5.41)$$

There is no electric charge factor outside the summation because, just as quarks form strong interaction isospin multiplets with different electric charges, the leptons also form weak isospin multiplets, but in this case the resulting weak charge is the same for all quarks.<sup>16</sup>

From Equation (5.40) and (5.41), we expect

$$F_2^{\nu N}(x) \leq \frac{18}{5} F_2^{\ell N}(x). \quad (5.42)$$

The experimental data illustrated in Figure 5.17 show that  $F_2^{\ell N}(x)$  and  $F_2^{\nu N}(x)$  are equal within errors except possibly at small values of  $x$  where antiquarks are more important. Thus one can conclude that the partons do have charges  $\frac{2}{3}$  and  $-\frac{1}{3}$ , which completes the evidence for identifying partons with quarks.

<sup>16</sup>Weak isospin will be discussed briefly in Chapter 6.

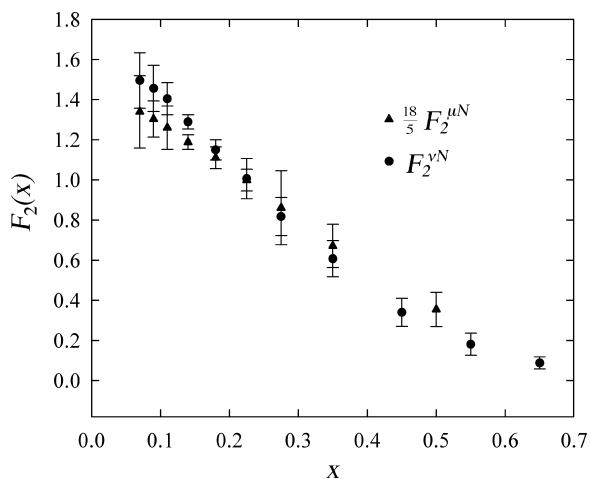


**Figure 5.17** Comparison of  $F_2(x)$  from deep inelastic muon (data from Ar97) and neutrino (data from Se97) scattering experiments; the data points are the average over a range of  $Q^2 > 2 (\text{GeV}/c)^2$  and the error bars express the range of data values within the  $Q^2$  ranges

Combining data from different experiments, with electrons, muons, neutrinos and antineutrinos as projectiles, enables individual quark/parton momentum distributions to be extracted from combinations of cross-sections. Some typical results at  $Q^2 = 10 (\text{GeV}/c)^2$  are shown in Figure 5.18 for the combinations

$$Q(x) = d(x) + u(x) \quad (5.43a)$$

and

$$\bar{Q}(x) = \bar{d}(x) + \bar{u}(x). \quad (5.43b)$$

The difference

$$Q_v(x) \equiv Q(x) - \bar{Q}(x) \quad (5.44)$$

can be identified as the distribution of the valence quarks of the quark model. It can be seen that  $Q_v$  is concentrated around  $x \approx 0.2$  and dominates except at small values of  $x$  where the antiquarks  $\bar{q}$  in the sea distribution are important.

The results of Figure 5.18 reveal an interesting and unexpected result concerning gluons within the nucleon. If we integrate the momentum distributions for quarks and antiquarks over all  $x$  we might expect to recover the total momentum of the nucleon, whereas the curves of Figure 5.18 yield a value of approximately 0.5. Thus it follows that about 50 per cent of the momentum is carried by gluons.

Although scaling is approximately correct, it is certainly not exact. In Figure 5.19 we show some deep inelastic scattering data plotted in more detail. The

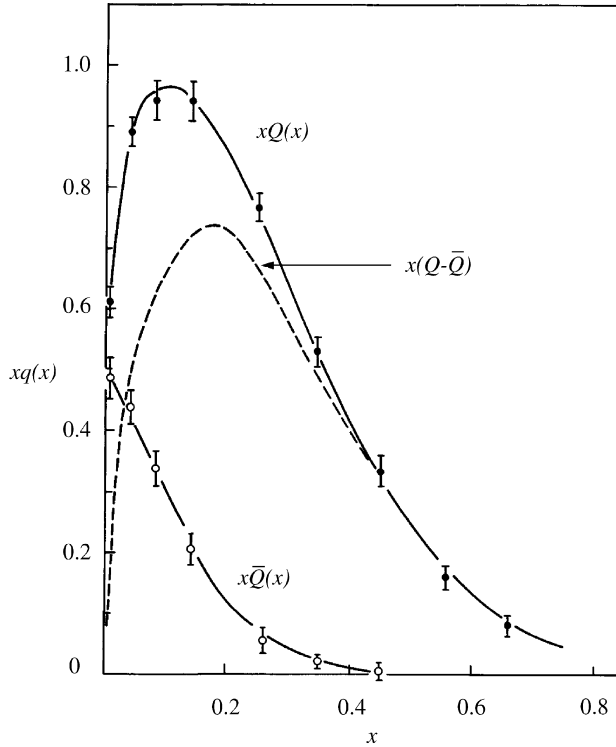
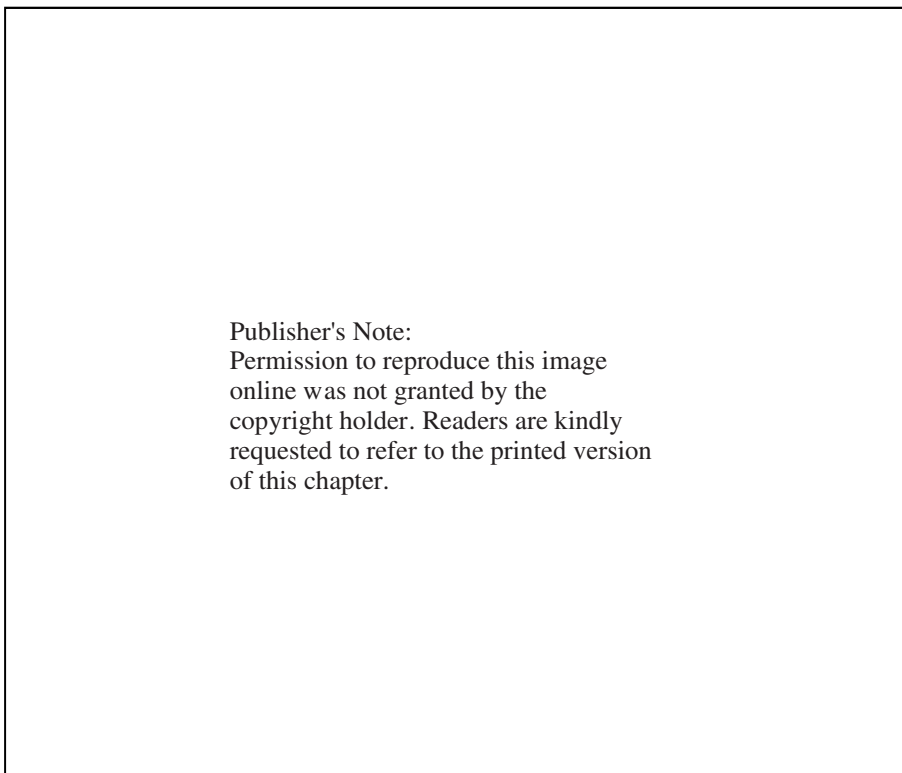


**Figure 5.18** Quark and antiquark momentum distributions in the nucleon

deviations from scaling are due to QCD corrections to the simple quark model, i.e. the quark in the proton that is struck by the exchanged photon can itself radiate gluons. Again, without further details, the scaling violations are explained by QCD using a value of the strong interaction parameter  $\Lambda$  that is consistent with that obtained from other sources (e.g. the three-jet events that we have discussed above).<sup>17</sup>

Finally, it is worth noting that the nucleon structure functions and hence the quark densities are found from lepton scattering experiments using a range of different nuclear targets. We have seen that the average binding energy of nucleons in heavy nuclei is of the order of 7–8 MeV per nucleon. As this energy is much smaller than those used in deep inelastic scattering experiments, it might be thought safe to ignore nuclear effects (except those due to the internal motion of the nucleons – the Fermi momentum – that are typically about 200 MeV/c). However, experiments have shown that the structure functions do in fact depend

<sup>17</sup>Scaling violations are discussed in detail, but at a more advanced level than here in, for example Ha84.



Publisher's Note:  
 Permission to reproduce this image  
 online was not granted by the  
 copyright holder. Readers are kindly  
 requested to refer to the printed version  
 of this chapter.

**Figure 5.19** A compilation of values of  $F_2$  measured in deep inelastic electron and muon scattering from a deuterium target -- different symbols denote different experiments; for clarity, the data at different values of  $x$  have been multiplied by the factors shown in brackets and the solid line is a QCD fit with  $\Lambda = 0.2$  GeV (adapted from Mo94, copyright the American Physical Society)

slightly on the nuclear medium. Although the effects are very small and not enough to alter the conclusions of this chapter, it is a reminder that there are still things to be learnt about the role of nuclear matter and that this may hold information on the nuclear force in terms of the fundamental quark–gluon interaction.

## Problems

- 5.1** The general combination of  $m$  quarks and  $n$  antiquarks  $q^m \bar{q}^n$ , with baryon number  $B > 0$  has a colour wavefunction that may be written  $r^\alpha g^\beta b^\gamma \bar{r}^\alpha \bar{g}^\beta \bar{b}^\gamma$ , where  $r^\alpha$  means that there are  $\alpha$  quarks in the  $r$  colour state, etc.. By imposing the condition of colour confinement, show that  $m - n = 3p$ , where  $p$  is a non-negative integer and hence show that states with the structure  $qq$  are not allowed.

- 5.2 Draw the lowest-order Feynman diagrams for the following processes:
- the interaction of a quark and a gluon to produce a quark and a photon;
  - the production of a single  $Z^0$ -boson in a collision of protons and antiprotons;
  - the annihilation of an electron and a positron to produce a pair of  $W$ -bosons.
- 5.3 A  $p\bar{p}$  collider with equal beam energies is used to produce a pair of top quarks. Draw a Feynman diagram for this process that involves a single gluon. If the three quarks of the proton (or antiproton) carry between them 50 per cent of the hadron total energy–momentum, calculate the minimum beam momentum required to produce the  $t\bar{t}$  pair.
- 5.4 The lowest Feynman diagram for inelastic electron–proton scattering at high energies

$$e^-(E, \mathbf{p}c) + p(E_p, \mathbf{P}_p c) \rightarrow e^-(E', \mathbf{p}'c) + X(\text{hadrons})$$

is shown in Figure 5.20.

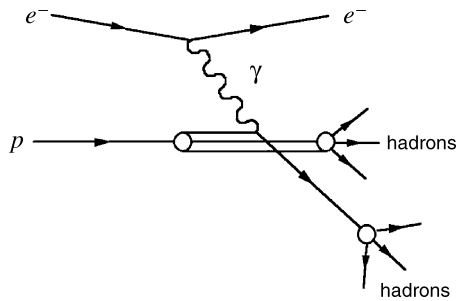


**Figure 5.20** Kinematics of inelastic electron–proton scattering

Use energy–momentum conservation to show that the variable  $\nu$  defined in Equation (5.24) becomes  $\nu = E - E'$  in the rest frame of the proton. Hence show that the variable  $x$  defined in Equation (5.25) lies in the range  $0 \leq x \leq 1$  if the mass of the electron is neglected.

- 5.5 If hadron–hadron total cross-sections are assumed to be the sum of the cross-sections between their constituent quarks, show that the quark model predicts the relationship:

$$\sigma(\Lambda p) = \sigma(pp) + \sigma(K^- n) - \sigma(\pi^+ p).$$

- 5.6 The  $3\gamma$  decay of positronium (the bound state of  $e^+e^-$ ) has a width that in QED is predicted to be  $\Gamma(3\gamma) = 2(\pi^2 - 9)\alpha^6 m_e c^2 / 9\pi$ , where  $\alpha$  is the fine structure constant. If the hadronic decay of the  $c\bar{c}$  bound state  $J/\Psi(3100)$  proceeds via an analogous

mechanism, but involving three gluons, use the experimental hadronic width  $\Gamma(3g) = 80 \text{ keV}$  to estimate the strong interaction coupling constant  $\alpha_s$ . Use an analogous assumption to estimate  $\alpha_s$  from the radiative width  $\Gamma(gg\gamma) = 0.16 \text{ keV}$  of the  $b\bar{b}$  bound state  $\Upsilon(9460)$ .

5.7 Use Equations (5.38) and (5.39) to derive the *Gottfried sum rule*,

$$\int_0^1 [F_2^{ep}(x) - F_2^{en}(x)] \frac{dx}{x} = \frac{1}{3} + \frac{2}{3} \int_0^1 [\bar{u}(x) - \bar{d}(x)] dx,$$

where the quark distributions refer to the proton.

5.8 Estimate the cross-section ratio  $R$  defined in Equation (5.20) at centre-of-mass energies  $E_{\text{CM}} = 2.8 \text{ GeV}$  and  $15 \text{ GeV}$ . How would  $R$  change if the energy were increased so that top quark pairs could be produced?

5.9 Common forms assumed for the momentum distributions of valence quarks in the proton are:

$$F_u(x) = xu(x) = a(1-x)^3; \quad F_d(x) = xd(x) = b(1-x)^3.$$

If the valence quarks account for half the proton's momentum, find the values of  $a$  and  $b$ .

5.10 The cross-section  $\sigma(u\bar{d} \rightarrow W^+)$  near the mass of the  $W^+$  is given by the Breit-Wigner form

$$\sigma = \frac{\pi(\hbar c)^2 \lambda^2 \Gamma_{u\bar{d}}}{3[4(E - M_W c^2)^2 + \Gamma^2]},$$

where  $(M_W, \Gamma)$  are the mass and total width of the  $W^+$ ,  $\Gamma_{u\bar{d}}$  is the partial width for  $W^+ \rightarrow u\bar{d}$ ,  $E$  is the total centre-of-mass energy of the  $u\bar{d}$  pair and  $\lambda = 2/E$ . Find the maximum value of  $\sigma$ , i.e.  $\sigma_{\text{max}}$ , given that the branching ratio for  $W^+ \rightarrow u\bar{d}$  is  $1/3$ . Use this result and the quark distributions of Question 5.9 to find an expression for the cross-section  $\sigma(p\bar{p} \rightarrow W^+ + \dots)$  in terms of the  $p\bar{p}$  total centre-of-mass energy  $\sqrt{s}$  and  $\sigma_{\text{max}}$  and evaluate your result for  $\sqrt{s} = 1 \text{ TeV}$ . (Use the narrow width, i.e. delta function, approximation

$$\sigma_{u\bar{d}}(E) = \pi \frac{\Gamma_W}{M_W c^2} \sigma_{\text{max}} \delta\left(1 - \frac{E^2}{(M_W c^2)^2}\right)$$

in integrals.)